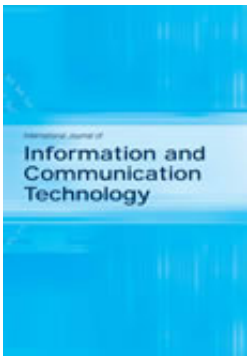

International Journal of Information and Communication Technology

ISSN online: 1741-8070 - ISSN print: 1466-6642
https://www.inderscience.com/ijict

Intelligent detection of rail transit vehicle wheelsets combined with structured light technology

Jun Ma, Xu Xue, Bingzhi Chen

DOI: 10.1504/IJICT.2025.10072557

Article History:

Received:	18 December 2024
Last revised:	15 May 2025
Accepted:	15 May 2025
Published online:	30 July 2025

Intelligent detection of rail transit vehicle wheelsets combined with structured light technology

Jun Ma*

Institute of Mechanical Engineering,
Dalian Jiaotong University,
Liaoning Dalian 116028, China
Email: majun_jdyz@163.com
*Corresponding author

Xu Xue

School of Electrical Engineering,
Dalian Jiaotong University,
Liaoning Dalian 116028, China
Email: xx888325@163.com

Bingzhi Chen

Institute of Mechanical Engineering,
Dalian Jiaotong University,
Liaoning Dalian 116028, China
Email: chenbingzhi06@126.com

Abstract: Real-time monitoring of rail transit vehicle wheelsets is of great significance to the stable operation and maintenance of packing vehicles. This paper aims to design a system that can accurately detect rail transit vehicle wheelsets in real time, improve the intelligent detection efficiency of rail transit vehicle wheelsets, and ensure the safety and efficiency of rail transit running. Aiming at the complex multi-line structured light (MLSL) fringe centre line extraction problem in the original image of the system, this paper studies the light fringe matching segmentation method based on blob analysis and the improved Steger centre line extraction algorithm. The test results show that the measurement accuracy of wheel diameter and rim width is ±0.2 mm, the measurement accuracy of rim width and height is ±0.25 mm, and the measurement error of QR value is less than 0.25 mm. The detection result curve of the system proposed basically coincides with the standard value, which shows that the measured results in this paper can be consistent with the standard value. Therefore, the system proposed provides some technical support for intelligent detection of rail transit vehicle wheelsets. The system proposed can also be extended to other rail transit industries.

Keywords: structured light technology; rail transit; vehicle wheelsets; intelligent detection.

Reference to this paper should be made as follows: Ma, J., Xue, X. and Chen, B. (2025) 'Intelligent detection of rail transit vehicle wheelsets combined with structured light technology', *Int. J. Information and Communication Technology*, Vol. 26, No. 30, pp.1–23.

Biographical notes: Jun Ma graduated from Dalian Jiaotong University At present, he is mainly engaged in research on intelligent sensing, measurement and control technology, and image recognition technology. He has participated in multiple projects in cooperation between Dalian Jiaotong University and CRRC China including digital debugging, testing system, and image recognition. He published multiple SCI, Chinese core, and technology core articles as the first author. He has participated in the Liaoning Provincial Transportation Science and Technology Project 'Research on intelligent diagnosis and performance degradation assessment of urban rail vehicle running parts' and the Liaoning Provincial Department of Education's Natural Science Research 'Research on multi terminal information transmission and debugging methods for Chinese standard EMU'.

Xu Xue graduated from Dalian Jiaotong University and is currently mainly engaged in engaged in comprehensive automation and advanced control technology. He participated in the Liaoning Provincial Transportation Science and Technology Project 'Research on intelligent diagnosis and performance degradation assessment of urban rail vehicle operating components' and the Liaoning Provincial Department of Education's Natural Science Research 'Research on multi terminal information transmission and debugging methods for Chinese standard EMU'. As the project leader, he has led the construction project of CRRC Tangshan Locomotive and Rolling Stock Co., Ltd.'s standard production line for high-speed trains over 250 kilometres – the integration of single vehicle debugging and testing platform and paperless automatic execution technical services.

Bingzhi Chen is a Professor who specialises in virtual prototype performance simulation, multidisciplinary optimisation design, and biomechanical research of rail vehicles. He has led multiple national level projects such as the National Natural Science Foundation and the National Key R&D Program, and has achieved breakthrough results in the fields of lightweight design for high-speed rail and passive safety protection for trains. Representative projects include the research and development of over 50 types of trains, such as CR400 high-speed trains and A-type subways, and have completed the optimisation design of nearly 8,000 train bodies and key components. As the project leader, he led the anti-collision analysis and optimisation of energy absorbing components for high-speed trains based on material and structural integration.

1 Introduction

Wheelset is the most important running component and supporting component of rail vehicle formed by connecting two wheels through axles, and it is the core component of transmission system. It not only bears all the weight from the whole carriage, but also bears large dynamic and static loads, wheel-axle assembly stress and thermal stress caused by wheel-rail friction during braking. The wheel tread is the outer circumferential surface where the wheel is in direct contact with the rail, and the wheelset rolls under the action of friction between the tread and the rail. For the absolute safety of driving, both newly produced train wheelsets and repaired wheelsets need accurate measurement.

Static detection refers to the measurement of the wheelset when the wheelset is separated from the car body or when the wheelset is not separated from the train body and the train is at rest. Dynamic online measurement technology has the advantages of

fast detection speed, high degree of automation, and no occupation of vehicle turnover time. Compared with dynamic measurement, static measurement does not need to consider the vibration generated when the train is running, and can uniformly and continuously measure the whole circumference section of the wheelset, which is easier to achieve higher measurement accuracy, and has comprehensive data. Moreover, it can measure the whole circumference measurement items that cannot be measured by dynamic measurement such as wheel diameter jump and end jump in the wheelset. It is not only suitable for the final inspection before the new wheelset is loaded, but also for the inspection after the wheelset is repaired (Jwo et al., 2021).

The manufacturing quality inspection method of rail train wheelset must be developed from mechanical measurement technology to electronic measurement method of overall error measurement and numerical control coordinate optical measurement method. The two-dimensional detection and evaluation method of wheelset section based on dots and lines cannot completely reflect the manufacturing information or defect wear condition of the whole wheelset tread, and the detection results are one-sided.

Combined with the development status of wheelset tread detection, the wheelset measurement and evaluation method considered in this paper adopts line structure measurement. Moreover, this paper combines reverse engineering to reconstruct the whole tread topography data in 3D, and detects the whole parameters of the train wheelset in 3D. This non-contact measurement method has the advantages of high precision, anti-interference, adaptability to various complex curved surfaces, etc. In addition, it can restore the original shape of the tread to the greatest extent and ensure the authenticity, reliability and stability of the measurement results.

2 Related works

2.1 Static detection

Mosleh et al. (2023) designed a contact detection device based on parallel telescopic mechanism, which used a fixed-length connecting rod to drive the rotating side head to scan and measure the surface of the tread, calculated the centre trajectory of the roller by obtaining the rotation angle of the measuring arm, and further obtained the surface tread profile. Guedes et al. (2023) adopted an automatic measuring device for contact measurement between the side head with natural diamond and the tread surface, which contacted the outer ring of the wheel bearing for positioning. Moreover, the system runs stably and has high measurement accuracy. The measurement process is completely controlled by the computer, thus realising the transformation of wheelset detection from manual to mechanical automation. For the contact measurement method, although it has strong anti-interference ability and high reliability of measurement results, its detection efficiency is low, and the contact part will be worn after long-term use.

Fu et al. (2023) proposed a photoelectric detection method for wheelset geometric parameters and tread defects, which used laser displacement sensor and CCD vision sensing technology to measure the main dimensional parameters of wheelset. In the process of slow rotation of the wheelset, a precise motion control mechanism is used to drive the sensor to quickly scan back and forth along the circumferential direction of the axle at an interval of 3 mm to locate the defects that may exceed the limit. The laser displacement sensor is then controlled to scan again only at the positioned defect at

intervals of 1 mm in the axial direction and 0.2 mm in the circumferential direction of the wheel. Finally, the measurement data are collected and processed to find the size of the defect.

2.2 Dynamic detection

Wheelset dynamic detection technology refers to the detection of wheelset when the vehicle is running. The dynamic measurement methods of wheelset comprehensive parameters mainly include ultrasonic telemetry, vibration detection, contact measurement, laser measurement and image measurement.

1 Ultrasonic telemetry method

Multiple ultrasonic telemetry sensors are used to measure the distance of the wheel surface, and the wheel size parameters are calculated by obtaining the detection data with the vehicle speed less than 5 km/h for processing and analysis. The device has fast detection speed and high accuracy, but its structure is relatively complex and is easily affected by the external environment (Guo et al., 2022).

2 Vibration detection method

When the wheel tread is damaged, the vibration and impact between the wheel and rail at the defective place during vehicle running is much larger than that at the non-defective place. The vibration detection method (Lourenço et al., 2024) uses the vibration acceleration sensor installed beside the railway track to detect the instantaneous impact load between the wheel and the rail, and then processes and analyses the data amplified by the charge amplifier to judge and measure the defect. This kind of device has convenient data acquisition and simple method, but the vibration signal acquisition is easily affected by the external environment, and there are deviations and noises, which makes the measurement accuracy and stability not high.

3 Contact measurement method

Shaikh et al. (2023) designed a wheelset detection device based on the principle of parallelogram mechanism. The laser displacement sensor installed on it can measure the dimensional parameters at any place of tread when the wheel is walking. This device has high measurement accuracy and good stability, but its detection mechanism is more complicated, and the error will accumulate in the process of processing and assembly. Moreover, the rail also has certain deformation, which makes the measurement benchmark deviate, and then causes the measurement error.

4 Laser measurement method

Peng et al. (2023a) proposed a dynamic measurement method of wheel tread, which used 26 independent displacement sensors to measure the wheel profile at different positions, and processed and analysed the measurement results of each sensor through the data processing system of the host computer to obtain the wheel geometric parameters. By building a sensor array, vehicles running at 45 mph can still be accurately measured. However, although the system can detect the wheel size at a high speed, it needs many sensors, and it is difficult to install and debug on site.

5 Image method

He et al. (2022) proposed a tread defect identification method based on GA-RBFNN algorithm by analysing the characteristics of tread defect geometry, texture and grey distribution, which used floating-point coding, GA crossover and mutation to optimise network parameters. Compared with traditional algorithms, the accuracy of defect identification is improved. The defect detection method based on texture clustering and region growth proposed in Su et al. (2024) uses grey level co-occurrence matrix to perform K-means++ clustering on the acquired variance, contrast, texture and other features to determine the damage region, and then introduces back propagation (BP) and support vector machine (SVM) to determine the tread damage. When the features extracted by this method cannot express all the defects, the generalisation ability of recognition will be poor, and the detection accuracy will be difficult to guarantee in practical applications (Peng et al., 2023b).

Dynamic online detection technology does not need to disassemble the wheelset. However, it has high requirements for installation accuracy, expensive equipment, easily affected by rail vibration, and can only measure part of the wheelset section, so it has not been widely used in the field (Zhu et al., 2020). Static detection does not need to consider the vibration generated when the train is running. Moreover, the measurement accuracy is high, the stability is good, and the detection data is more comprehensive. For the measurement of parameters such as tread abrasion and spalling, its application scope is limited (Velletrani et al., 2020). However, object detection methods based on deep learning have high recognition accuracy and fast speed, and are widely used in a variety of industrial detection fields, so they have broad prospects (Li et al., 2022).

This paper designs a wheelset comprehensive parameter detection device based on line SL. The line SL technology is used to measure the overall dimension parameters of the wheelset, and the deep learning target detection network is combined to detect the defects of the tread, so as to realise the automatic measurement of the wheelset comprehensive parameters.

3 System design

It is necessary to screen a series of pixels in the light fringe to restore the contour information of tread surface. Whether the selected feature points are accurate or not will affect the accuracy of measurement results. The light fringe can be extracted, and the brightest centreline point with stronger anti-interference ability in the fringe can be taken as the feature point.

3.1 Analysis of light fringe centreline extraction algorithm

The schematic diagram of the MLSL source is shown in Figure 1. The modulated point light source is projected into a special MLSL diffractive optical element (DOE), and through the diffraction modulation of DOE, multiple SL fringes with mutually parallel, uniform width, same length and similar grey distribution are obtained.

Figure 1 Internal schematic diagram of multi-line laser (see online version for colours)

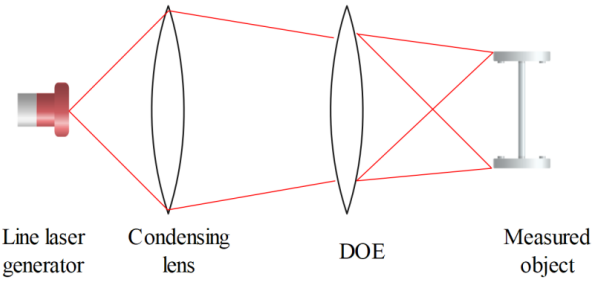

The centreline extraction methods can be divided into pixel-level and sub-pixel-level extraction methods according to the extraction accuracy. The pixel-level extraction algorithm is simple in principle and fast in extraction speed, but its accuracy is relatively low. Grey distribution and other factors, and the extraction accuracy is higher, but the extraction speed of this method is slow. The centreline extraction algorithm needs to be selected for different application scenarios and measurement requirements.

1 Threshold method

The greyscale value on the cross section is symmetrically distributed on both sides of the centreline. This method determines the boundary positions p and q of the LS on the cross section by selecting a suitable threshold (Mohammadi et al., 2023).

$$c = (p+q)/2 \tag{1}$$

The method is simple in principle and small in computation. However, the anti-interference ability of image noise is not high, and the accuracy is low.

2 Directional template method

This method originates from the idea of greyscale centre. When the shape of the LS changes due to the surface change of the measured object, in a very small range, there are only four directions of the LS extending: horizontal, longitudinal, left oblique 45° and right oblique 45°. This algorithm combines the idea of template operation and the direction transformation of light fringes, which effectively reduces the influence of noise and has the ability to repair disconnection, but it needs to calculate all pixels in the graph, which requires a large amount of calculation and only has pixel-level accuracy. For light fringes with obvious width change, the extraction effect is poor.

3 Skeleton extraction method

Skeleton extraction method is a binary morphological refinement method. In this method, the pixels of binarised light fringes are divided into contour pixels and skeleton pixels by setting appropriate judgement conditions, and the contour pixels are removed by iterative algorithm to obtain the central skeleton line with single pixel width, which keeps the connectivity and topological characteristics of light fringes. This method can ensure the continuity of the centreline, and has good stability and accuracy. Moreover, with the emergence of methods such as fast look-up tables, the extraction speed has been rapidly improved.

4 Grey centre of gravity method

If it is assumed that after the image is preprocessed, the interval and the light bar in the i^{th} row is located is $[m, n]$, then the centre point V_i of the line change is (Sun et al., 2023):

$$V_i = \sum_{k=m}^{n} k * I_k \Big/ \sum_{k=m}^{n} I_k \tag{2}$$

In the formula, I_k is the greyscale value of the k^{th} pixel in the i^{th} row. The grey centre of gravity method has a fast calculation speed, can obtain the sub-pixel centre line, and has a good extraction effect when the greyscale of the light bar is not strictly symmetrical. However, when calculating the centreline, the centreline extraction is carried out row by row, and the accuracy is low under the condition of large curvature change of fringe and strong noise interference.

5 Curve fitting method

The principle of curve fitting method is to analyse the grey value distribution law of one row or column on the light bar, use an appropriate function to fit the grey change curve, and select the maximum point of the function as the centre of the LS. According to the variation law of LS, polynomial and Gaussian function can be used to fit the grey variation curve of LS. According to the characteristics of the selected light source, Gaussian function is used for fitting. The grey values are assumed to conform to a Gaussian function (Ren et al., 2022):

$$g(x) = A\exp\left[-B(x - x_0)2\right] \tag{3}$$

By taking the logarithm of both sides, the following result is obtained:

$$\begin{cases} \ln[g(x)] = a_0 + a_1 x + a_2 x^2 \\ a_0 = \ln A - Bx_0^2 \\ a_1 = 2Bx_0 \\ a_2 = -B \end{cases} \tag{4}$$

By bringing the points on the light cross section into formula (4), a_0, a_1, a_2 are obtained, and the centre point position can be obtained:

$$x_0 = -\frac{a_1}{2a_2} \tag{5}$$

In this method, suitable functions can be selected for fitting according to different light sources, and the sub-pixel centre point can be obtained. However, it is necessary to curve fitting the greyscale of each row/column during calculation, and the computational complexity is high.

3.2 Improved Steger algorithm based on skeleton pre-extraction

The Steger algorithm can solve the centreline with sub-pixel accuracy, and it has a good effect on extracting light streaks with large curvature changes. However, the Steger algorithm needs to perform multiple convolution calculations on all pixels, and the extraction efficiency is low.

The curvature of light fringe changes greatly. Considering comprehensively, the improved Steger algorithm is selected as the centreline extraction algorithm proposed to improve the measurement accuracy of the system. The skeleton extraction method is used to pre-extract the pixel-level centreline of light fringe, and then the Steger algorithm is used to accurately calculate the sub-pixel centreline of light fringe.

The main steps of the Steger algorithm are as follows: first, according to the fringe width in the image, a suitable Gaussian kernel function is set to convolve the image to obtain the Hessian matrix $H(x, y)$ of the light bar image (Kaliorakis et al., 2023):

$$H(x, y) = \begin{bmatrix} h_{xx} & h_{xy} \\ h_{xy} & h_{yy} \end{bmatrix} \tag{6}$$

Among them, h_{xx}, h_{xy} and h_{yy} are obtained by convolving the original image y with the template made by the Gaussian kernel function based on the scale space theory:

$$h_{xx} = \frac{\partial^2 g(x, y)}{\partial^2 x} \otimes I(x, y) \tag{7}$$

$$h_{xy} = \frac{\partial^2 g(x, y)}{\partial x \partial y} \otimes I(x, y) \tag{8}$$

$$h_{yy} = \frac{\partial^2 g(x, y)}{\partial^2 y} \otimes I(x, y) \tag{9}$$

Among them, $\otimes$ represents the convolution operation, and $g(x, y)$ satisfies:

$$g(x, y) = -\frac{1}{2\pi\delta^2} e\left(-\frac{x^2 + y^2}{2\delta^2}\right) \tag{10}$$

Secondly, the normal vector (n_x, n_y) of each point in the image is obtained by performing eigenvalue decomposition on $H(x, y)$. In the LS, this direction is the cross-sectional direction of the LS. Moreover, a second-order Taylor expansion is performed along the normal line at a point (x_0, y_0) in the LS to obtain the greyscale distribution function $s(t)$ of the LS at any position $(x_0 + tn_x, y_0 + tn_y)$ in this direction (Bruni et al., 2022):

$$s(t) = s\left(x_0 + tn_x, y_0 + tn_y\right) = I\left(x_0, y_0\right) + N\left(h_x, x_y\right)^T + NH(x, y)N^T/2 \tag{11}$$

$N = (tn_x, tn_y)$ is the distance h_x from a point on the cross section to (x_0, y_0), and x_y is the first-order derivative of the point, which can be obtained by formula (12):

$$\begin{cases} h_x = \dfrac{\partial g(x, y)}{\partial x} \otimes I(x, y) \\ h_y = \dfrac{\partial g(x, y)}{\partial y} \otimes I(x, y) \end{cases} \tag{12}$$

By setting $\dfrac{\partial s}{\partial t} = 0$, we can get:

$$t = \frac{n_x h_x + n_y h_y}{n_x^2 h_{xx} + 2 n_x n_y h_{xy} + n_y^2 h_{yy}} \tag{13}$$

The coordinates of the sub-pixel centreline point are ($x_0 + tn_x$, $y_0 + tn_y$). In the actual operation process, each pixel in the image can obtain a centreline point through the Steger algorithm. Therefore, in the actual solution, the sum of greyscale value (tn_x, tn_y) $\in$ [–1/2, 1/2] × [–1/2, 1/2] is generally used as conditions to solve the accurate sub-pixel centrepoint.

From the solution process of the Steger algorithm, the algorithm performs five large-scale two-dimensional convolution operations on any point in the image to solve h_{xx}, h_{xy}, h_{yy}, h_x, h_y in the Hessian matrix of each pixel point, and its operating efficiency is low (Vrba, 2023).

Firstly, the pixel-level centreline of SL is obtained by skeleton extraction, and then the sub-pixel centreline is solved by using Steger algorithm at each point of the pixel-level centreline. The algorithm flowchart is shown in Figure 2.

Figure 2 Flowchart of improved Steger calculation based on skeleton pre-extraction

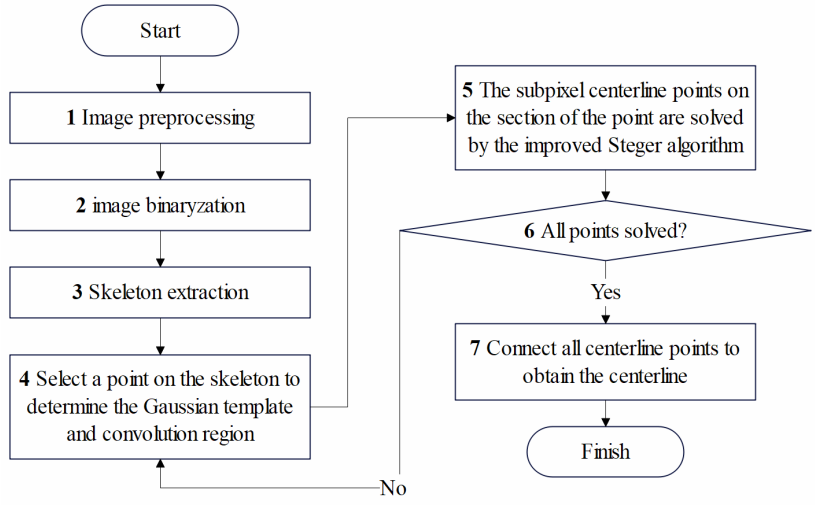

The light streak image after segmentation and matching is set to $f(x, y)$, and the corresponding binary image $g(x, y)$ can be obtained by image threshold segmentation.

The skeleton extraction method is to divide the foreground points in $g(x, y)$ into non-contour points and contour points through some judgement conditions, and delete all

contour points through multiple iterations. The remaining pixel-wide curve is the skeleton.

In a binarised image $g(x, y)$, the most associated pixels with a pixel are its surrounding pixels, which constitute the neighbourhood of the pixel. The definition of any pixel p_i and its eight neighbouring pixels p_2–p_9 is shown in the figure. When p_i is the foreground, its neighbourhood can be analysed to determine whether to retain p_i. All points in the image are traversed in a loop to remove non-skeleton points until the skeleton line is obtained.

Through skeleton extraction, the pixel-level centreline of light fringe is obtained, which is composed of a series of connected pixels. Then, the improved Steger algorithm is used to calculate these pixels one by one, and the sub-pixel intersection point of the cross section passing through each pixel and the centreline-centreline point can be obtained. By fitting them into a curve, the high-precision centreline can be obtained.

Figure 3 Pixel p_i and its neighbourhood

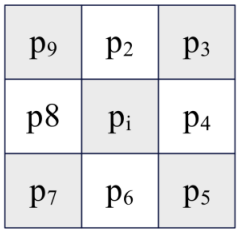

The specific solution algorithm flow is as follows (Song et al., 2024):

Step 1 The pixel-level centreline point extracted by the skeleton extraction method is p_1–p_n. The mean square error σ of the Gaussian function and the Gaussian template size $(2N + 1) \times (2N + 1)$ are calculated by the width of the stripes in the image to generate the Gaussian templates corresponding to the five first- and second-order partial derivatives of the image: S_x, S_y, S_{xx}, S_{yy}, S_{xy}. Corresponds to step 3 in Figure 2.

Step 2 The algorithm selects any point P_i in the skeleton point, and divides the image region Q with a size of $(2N + 1) \times (2N + 1)$ and a coordinate range of $[x_i - N: x_i + N: y_i - N: y_i + N]$ around $P_i(x_i, y_i)$ in the light streak image. Corresponds to step 4 in Figure 2.

Step 3 The algorithm performs an effective convolution operation on the five Gaussian templates of the Gaussian partial derivatives with Q to calculate the first and second order partial derivatives of the original image greyscale at P_i: $h_{xx}(x_i, y_i)$, $h_{xy}(x_i, y_i)$, $h_{yy}(x_i, y_i)$, $h_x(x_i, y_i)$, $h_y(x_i, y_i)$.

Step 4 The algorithm solves the Hessian matrix of P_i through formula (6), calculates the normal direction (n_x, n_y) of the point, solves the Taylor expansion of the point on the cross section through formula (11), and solves the sub-pixel offset t_i through formula (13), and finally solves the sub-pixel centreline point P_i' on the cross section corresponding to the point:

$$P_i' = \left(x_i + t_i n_x, y_i + t_i n_y\right) \tag{14}$$

Steps 3 and 4 correspond to step 5 in Figure 2.

Step 5 The algorithm determines whether all skeleton points have been solved. If all skeleton points have not been solved, the algorithm returns to step 2.

Step 6 The algorithm connects the sub-pixel centreline points together to obtain the sub-pixel level centreline. Corresponding to steps 6 and 7 in Figure 2.

4 Calibration method

4.1 Vehicle wheelset intelligent detection system

When using MLSL to measure the tread profile of a wheelset, it is necessary to build a visual sensor consisting of a MLSL laser and a camera next to the wheelset, as shown in Figure 4. The transformation matrix from the pixel coordinate system to the world coordinate system can be established by calibrating the camera and the MLSL plane. The MLSL is projected on the wheelset to form a plurality of light bars containing contour information. The camera photographs the light bars and extracts the contour information. Through the coordinate system transformation matrix, the contour of the wheelset can be restored to obtain a plurality of wheelset contour information.

Figure 4 Principle of measuring tread profile using MLSL

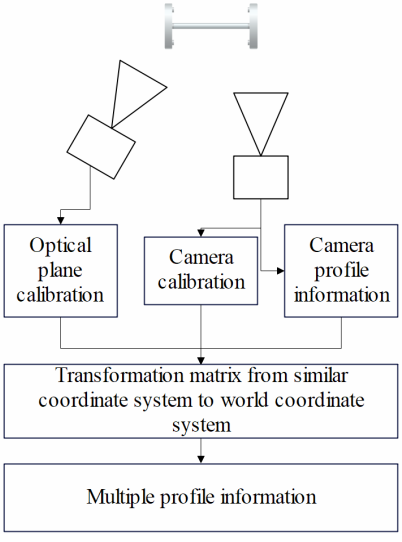

The scheme flow of the MLSL measurement system proposed is shown in Figure 5. The multi-line laser projects multiple light planes in space at a certain angle. The laser light strip will be modulated by the change of the surface profile of the measured object, captured by the camera at another position. The image processing of the collected light strip is carried out by computer software MATLAB, the pixel coordinates are converted into three-dimensional coordinates in the camera coordinate system.

Figure 5 Measurement system scheme (see online version for colours)

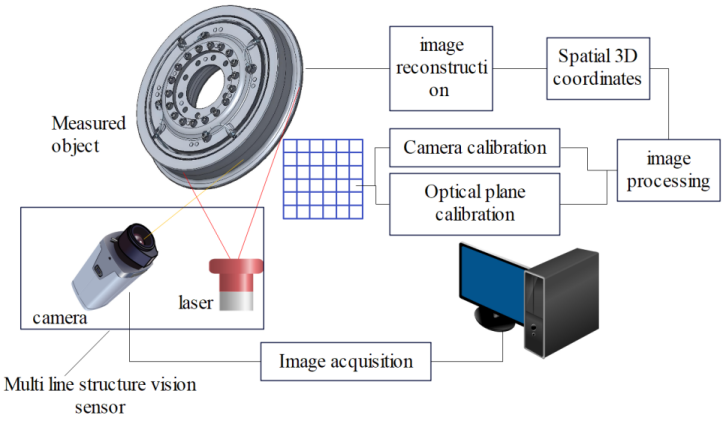

The basic structure of the wheelset diameter measurement system based on MLSL proposed is shown in Figure 6. The device adopts two sets of MLSL vision sensors, each of which has a camera and a MLSL laser. The two sets of sensors are mounted symmetrically outside the track at the centre position of the measured wheelset in the figure. When the measured wheelset passes through the positioning position shown in Figure 6, the photoelectric switch is triggered, and the MLSL vision sensor collects the wheelset image to obtain the wheelset contour image including a plurality of laser light bars as shown in Figure 7.

Figure 6 Wheelset diameter measuring system device (see online version for colours)

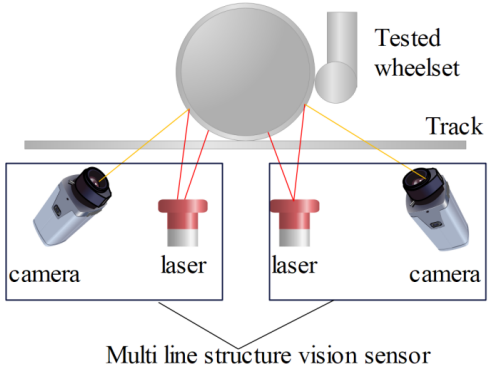

The two sets of devices can respectively obtain multi-light strip contour images on the left and right sides of the wheel, process the light strips in the images, synchronise the calibration results with the camera ray equation, realise image fusion, calculate the three-dimensional contour diagram of the wheelset tread to obtain the wheelset diameter, compare it with the actual measurement result, analyse the measurement error and improve it, so that the measurement system can complete the measurement of the wheelset diameter. The measurement method of MLSL vision sensor on one side is studied.

Figure 7 The multi-light strip image obtained by shooting

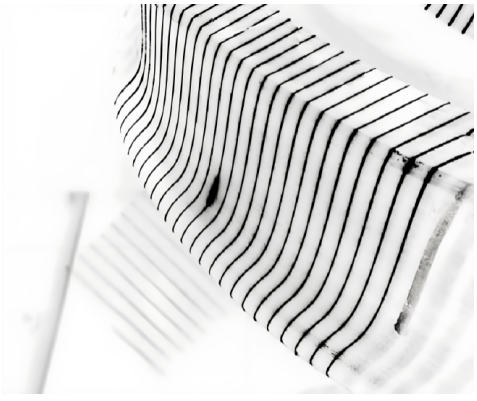

4.2 NURBS surface interpolation reconstruction method of tread

In essence, the interpolation reconstruction of NURBS surface is based on the two-parameter curve interpolation reconstruction in the horizontal and vertical directions. Firstly, the cross-section curve is reconstructed in one parameter direction, and then interpolated in the other parameter direction, so that the interpolation reconstruction of the whole surface is obtained.

The NURBS surface interpolation reconstruction process of wheelset tread is shown in Figure 8.

Figure 8 NURBS surface reconstruction flow chart

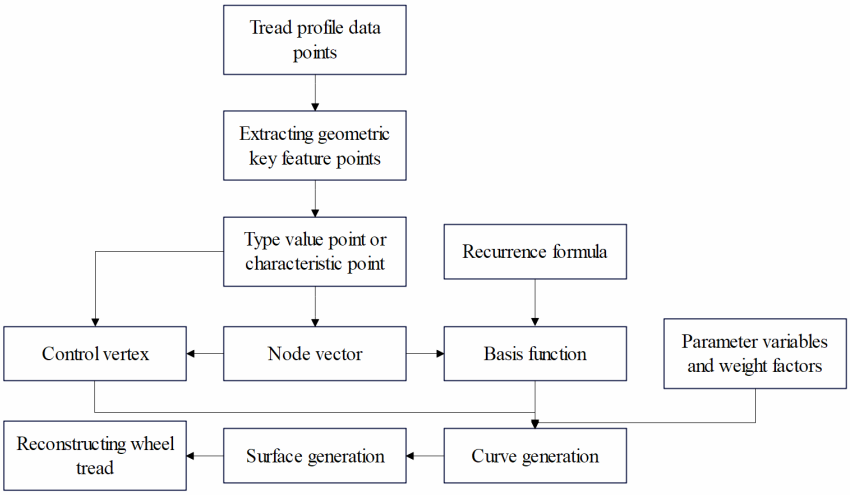

Firstly, the wheel tread section line point cloud data of the standard CRH5 wheel processed by data is reconstructed by NURBS curve interpolation for three times, and all section line control vertices are calculated according to this method, as shown in Figure 9.

Figure 9 Tread control vertex (see online version for colours)

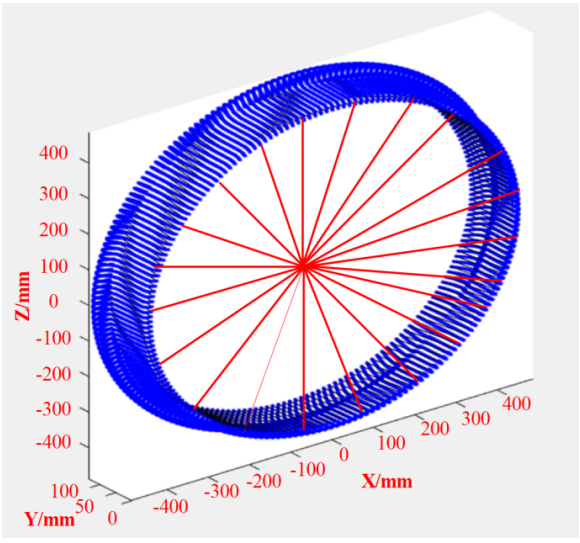

The control vertices of the generatrix cross-section lines of each wheel tread obtained above are used as reference value points in the circumferential direction, and the control vertices are back-calculated in the circumferential direction to obtain the control vertices of the entire tread and construct the NURBS surface.

4.3 Experimental methods

The standard wheelset of CRH5 trailer used in the experiment is tested by professional quality department, and its diameter is ∅890.12 mm, rim width is 135.05 mm, rim height is 28.92 mm, rim thickness is 32.36 mm, and QR value is 10.35 mm. The sensors used in the detection system are calibrated with the wheel diameter parameter value. The left and right sensors are installed at an angle of 20.15° to the vertical direction, and the calibration coefficient after positioning error compensation in the depth direction is K = 250. The experimental bench uses a servo motor to drive a 40 reduction ratio reducer to drive the chuck and wheelset to rotate at a constant speed of 5 r/min, so that the wheelset can rotate more than one round, and the data of one round of the middle rotation is selected. The encoder sends out 600 pulse commands, and at the same time, the double-line SL collects 600 tread section point cloud data, that is, the double-line SL sensor collects data every 0.6° rotation of the wheelset.

Based on the MLSL measurement system device proposed, the real-time detection experiment of wheelset is carried out. The overall process of the experiment is shown in Figure 10.

The SL measurement of wheelset tread is shown in Figure 11. Because only a one-sided probe system is built on the experimental platform, after the system calibration is completed with one wheel, the wheelset is withdrawn from the detection position, rotated by 180° and then put into the detection position, and then the measurement experiment is carried out on the other wheel of the wheelset. In order to improve the repeated measurement accuracy of the measurement system and compare the experimental results, multi-group measurements of the detection system and the fourth checker are carried out

on the wheelset to be measured. In this paper, the image and data processing are based on MATLAB R2021a software, which is good at correlation operation on matrix and array and meets the requirements of coordinate relationship transformation in this paper.

Figure 10 Flowchart of real-time detection of wheelset

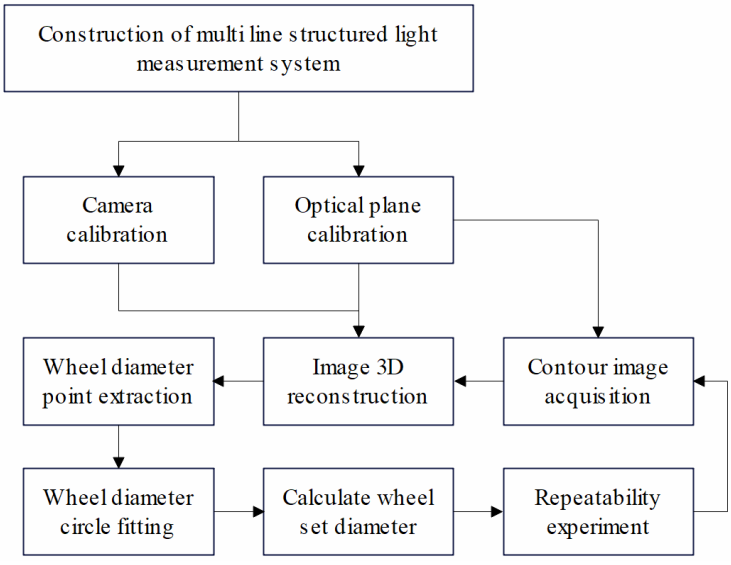

Figure 11 SL measurement of wheelset tread (see online version for colours)

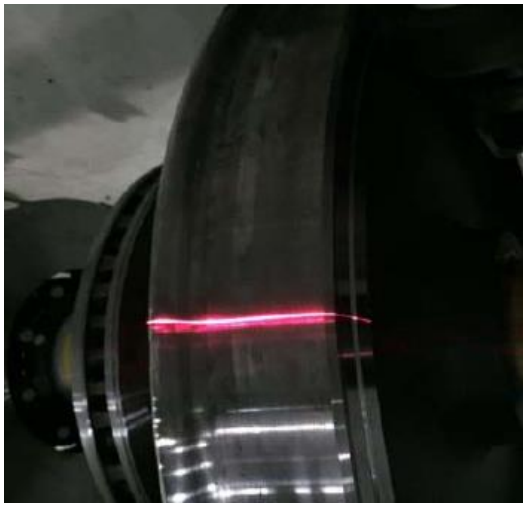

4.4 Experimental results

The geometric parameters of the wheelset are repeatedly measured and calculated by two measurement methods, and the results are sorted out as shown in Tables 1 and 2.

Table 1 Measurement results of wheelset measurement system (unit: mm)

Number of measurements	*Wheel diameter (D)*	*Rim width (L)*	*Rim height (H)*	*Rim thickness (W)*	*QR value*
1	890.08	135.17	28.96	32.51	10.45
2	889.93	135.05	28.89	32.45	10.37
3	890.04	135.06	29.01	32.56	10.42
4	890.00	135.09	28.78	32.41	10.35
5	889.88	134.97	28.79	32.49	10.29
6	890.10	135.02	28.91	32.45	10.48
7	890.03	135.08	29.02	32.58	10.33
8	889.98	134.98	28.88	32.52	10.38
AVE	890.02	135.05	28.91	32.49	10.38
STD	0.07	0.06	0.09	0.06	0.06

Table 2 Measurement results of the fourth inspector (unit: mm)

Number of measurements	*Wheel diameter (D)*	*Rim width (L)*	*Rim height (H)*	*Rim thickness (W)*	*QR value*
1	890.31	135.26	28.88	32.52	10.25
2	889.88	135.35	28.74	32.26	10.36
3	890.24	135.18	28.78	32.68	10.29
4	889.78	135.32	28.85	32.29	10.21
5	890.02	134.88	29.11	32.31	10.25
6	890.28	135.21	28.76	32.39	10.19
7	890.37	135.15	29.09	32.61	10.38
8	889.69	134.95	28.69	32.29	10.36
AVE	890.07	135.16	28.86	32.42	10.29
STD	0.26	0.17	0.16	0.16	0.07

By extracting the radial runout and end runout data, the pitch runout and end runout results are obtained as shown in Figure 12. The results show that the radial runout and end runout values of the wheel are both less than 0.04 mm.

To further verify the intelligent detection effect of the proposed model on vehicle wheelsets, the models of Peng et al. (2023a, 2023b) are used as controls to measure the wheel diameters and compare the measured results with the standard values to verify the accuracy of these methods. The measured results are expressed in the form of statistical graphs (Figure 13).

In order to verify the practicability of wheelset size measurement system based on multi line structured light in complex environment, a comparative test scheme including the influence of ambient light interference and mechanical vibration was designed. The baseline measurement was carried out in the laboratory standard environment (dark room, no vibration), and the reference values of wheel set diameter, rim thickness and other parameters were obtained as the control group. Set ambient light interference group and mechanical vibration group. The ambient light interference group uses adjustable light sources to simulate different light intensities (500–100,000 LX), covering cloudy to strong sunlight scenes, and adds high-frequency flickering light sources (frequency 50–100 Hz) to simulate dynamic interference. The mechanical vibration group is realised

by building a vibration platform to simulate the train running vibration (frequency 5–50 Hz, amplitude 0.1–2 mm), including the combined working conditions of periodic vibration and random shock

Figure 12 Calculation of radial runout and end runout, (a) wheel radial runout data (b) wheel end runout data (see online version for colours)

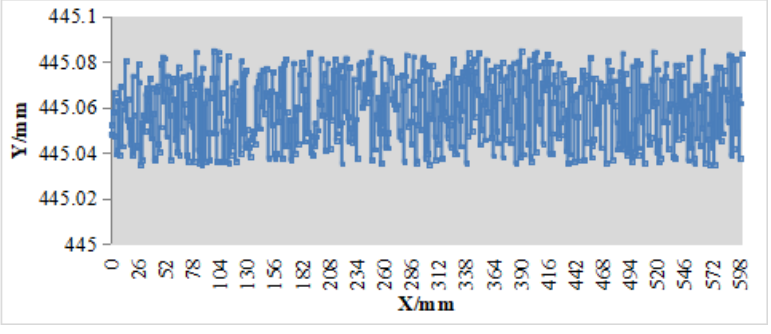

(a)

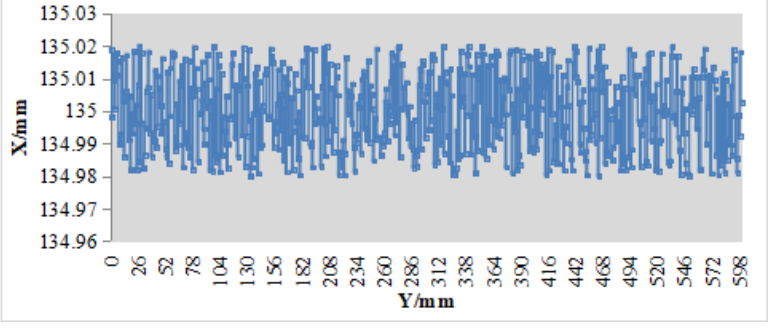

(b)

Each group was repeated 30 times with random interval. Synchronously collect ambient light intensity (illuminometer) and vibration spectrum (acceleration sensor) data. The test group data under standard environment are shown in Table 3.

Table 3 control group (standard environment)

Measurement parameters	*Mean (mm)*	*Standard deviation (mm)*	*Maximum error (mm)*
Wheel diameter	915.32	±0.08	–1.2
Rim thickness	32.45	±0.06	–1.125

Table 4 Environmental light interference group

Interference conditions	*Wheel diameter standard deviation (mm)*	*Mismatching rate of light stripes (%)*	*Invalid data frame ratio (%)*
Illumination 500 lx	±0.09	0.7	0.5
Illumination 80,000 lx	±0.11	1.2	2.8
Flash 100 Hz	±0.10	1.8	3.5

Figure 13 Comparison of detection results between the method proposed in this paper and existing studies (see online version for colours)

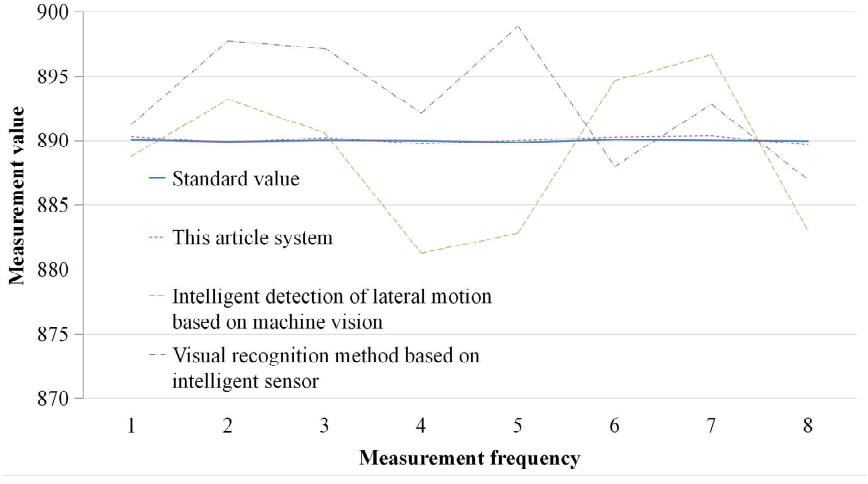

Table 5 Mechanical vibration group

Vibration condition	*Wheel diameter standard deviation (mm)*	*Outer surface fitting error (mm)*	*System reset time (ms)*
Sinusoidal vibration (20 Hz/1 mm)	±0.12	0.07	160
Random impact (acceleration 50 g/6 ms)	±0.15	0.09	190
Composite vibration (30 Hz + random impact)	±0.14	0.1	205

Using precision time protocol (PTP) to synchronise the clocks of the camera, vibration platform, and processing terminal (with an accuracy of ±1 μs), the time parameters in the experiment were statistically analysed, mainly including: data acquisition delay – the time from the completion of light stripe exposure to the transmission of the image to memory; algorithm processing time: including the entire process of light stripe extraction, 3D reconstruction, and parameter calculation; system reset delay: the time when an abnormal state returns to steady-state measurement after vibration shock.

The delay and processing time obtained on this basis are shown in Table 6.

Table 6 Delay and processing time statistics

Test conditions	*Data collection delay (ms)*	*Algorithm processing time (ms)*	*Total latency (ms)*
Control group (standard environment)	2.1 ± 0.3	14.2 ± 1.5	16.3
Strong light interference (80,000 lx)	2.3 ± 0.4	15.8 ± 2.1	18.1
Sinusoidal vibration (20 Hz/1 mm)	2.7 ± 0.6	16.5 ± 3.2	19.2
Random impact (50 g/6 ms)	3.5 ± 1.2	18.9 ± 4.7	22.4

Further verify the impact of out of roundness on accuracy, and the experimental sample configuration is shown in Table 7.

Table 7 Experimental sample configuration for the influence of non-roundness on accuracy

Non-roundness level	*Radial jump value (mm)*	*Number of polygon edges*	*Number of samples*
Standard roundness	≤0.05	-	5
Mild roundness	0.05–0.15	18–20 sides	5
Severe roundness	0.15–0.30	6–8 sides	5

The comparison of measurement data is shown in Table 8.

Table 8 Measurement data on the influence of non-roundness on accuracy

Measurement parameters	*Standard roundness group (σ/mm)*	*Mild non-circular group (σ/mm)*	*Severe non-circular group (σ/mm)*
Wheel diameter	±0.08	±0.12	±0.18
Rim thickness	±0.06	±0.09	±0.14
Flatness of outer surface	±0.04	±0.07	±0.11

4.5 Analysis and discussion

Facing the problem of intelligent detection of wheel profile wheelsets, proposes a method based on SL vision, aiming at improving the real-time monitoring efficiency and maintenance effect of rail transit vehicle wheelsets.

After analysing the camera imaging model, line SL measurement model and MLSL measurement model, the module, overall layout and workflow design of the wheelset dimension measurement system based on MLSL are completed, and the structure design, hardware selection and measurement model of the measurement module are emphatically studied.

Moreover, a three-dimensional measurement algorithm of wheelset size based on MLSL profile point cloud is studied. According to the characteristics of MLSL three-dimensional contour point cloud and wheel structure characteristics of wheel set, the flow of three-dimensional wheelset dimension measurement is given, and the wheel set dimension measurement is divided into wheel diameter and wheel rim parameter measurement. The cross-section curve of light plane and wheelset is studied, and the complete normal cross-section profile curve is obtained by rotating axis and auxiliary plane, and the measurement of rim parameters is completed.

According to the system design, a wheelset size measurement system based on MLSL is built, and the parameters of camera, MLSL plane and each measurement module are calibrated, and the three-dimensional measurement model of the system is constructed. After the laboratory preliminary verification that the detection accuracy and consistency meet the requirements, the system is installed in the field for further inspection, and the measurement accuracy comparison and repeatability analysis are carried out between the measurement results of the system and the manual measurement values, which verifies that the image processing algorithm and parameter measurement algorithm meet the detection requirements of the measurement system, and has certain feasibility.

In addition, in this paper, a fast MLSL plane calibration method suitable for general situations is proposed. No matter what angle the multi-line laser is projected on the surface of the object, only the first and last two light plane equations need to be calibrated in advance, and the rest of the light plane equations can be calculated at one time by the established MLSL measurement model, which reduces the process of image processing. Considering the influence of laser manufacturing process and environmental conditions, there will be deviation in the ideal situation of equal distance between projected light bars. Therefore, in this paper, the method of calculating the actual distance is extracted by extracting the coordinates of projection points of each light on the surface of the object. According to the geometric constraint relationship in the model, the normal vector of each light plane is calculated by Rodriguez function, and then the equation of each light plane is obtained.

Figure 12 shows that the measurement results meet the requirements of wheelset detection in railway departments, and the wheelset parameter results obtained by wheelset measurement system and manual measurement have certain deviations, but the overall measurement results of wheelset measurement system are better than manual measurement and are within the allowable range of measurement error. Among them, the measurement accuracy of wheel diameter and rim width is ±0.2 mm, the measurement accuracy of rim width and height is ±0.25 mm, and the measurement error of QR value is less than 0.25 mm.

The test result curve in Figure 13 basically coincides with the standard value, indicating that the measured results in this paper can be consistent with the standard value, and the test results are relatively accurate. The models in Peng et al. (2023a) and Velletrani et al. (2020) have large errors in this wheel detection, and it can be seen from the figure that the curve fluctuates greatly. Therefore, the reliability of the model proposed in this paper is further verified by comparison.

In Table 4, under 80,000 LX strong light, the light stripe mismatch rate only increased to 1.2%, and the standard deviation remained within ±0.11 mm, indicating that the improved Steger algorithm effectively suppressed the effect of high light overexposure through Gaussian filtering and adaptive threshold adjustment. The proportion of invalid data frames caused by flash frequency (100 Hz) is 3.5%, which is lower than the 5% threshold set by the system, thanks to the global shutter and exposure synchronisation control technology of CMOS sensor

In Table 5, the fitting error of the outer side under sinusoidal vibration (20 Hz) is only 0.07 mm, indicating that the plane fitting algorithm based on RANSAC has good robustness to low-frequency periodic vibration. The system reset time after random impact is 190 MS, which meets the requirements of real-time measurement in industrial scenes (<200 MS)

From the comparison of the variation range of the standard deviation between the control group and the interference group, the fluctuation range of the standard deviation of wheel diameter measurement was only expanded by 37.5% (±0.08 → ±0.15 mm), which was lower than the preset threshold of 150% The extraction time of light stripe centreline is stable at 15 ± 2 ms, which shows that the algorithm optimisation avoids the iterative divergence caused by dynamic interference

In Table 6, the strong light led to an increase in the number of iterations of the adaptive exposure control module (average+2 times/frame), which increased the processing time of the algorithm by 11.3% Through the hybrid strategy of fixed exposure mode and dynamic adjustment mode, the total delay under strong light is controlled

within 20 ms. The image blur caused by vibration makes the number of iterations of light stripe extraction fluctuate (15–22 times), but the improved algorithm limits the maximum processing time of a single frame to 25 ms through the pre convergence decision mechanism. The communication jitter caused by vibration impact increases the data acquisition delay by 66%, but the hardware level DMA transmission still ensures that 95% of the frame data completely reaches the processing unit. In general, the time benchmark performance of the system in complex environments fully meets the requirements of rail transit dynamic detection.

In Table 8, when the diameter jump value is >0.15 mm, the standard deviation of wheel diameter measurement reaches 180% of the nominal accuracy (0.1 mm), which is beyond the tolerance range of the system design. The iteration times of the improved algorithm under severe out of roundness conditions increase by 35%, but the plane fitting error is controlled within ±0.11 mm through the grouping sampling mechanism.

On the whole, the intelligent detection system of rail transit vehicle wheelset combined with SL technology proposed in this paper can effectively adapt to the operation needs of modern rail transit and meet the technical requirements of relevant departments.

5 Conclusions

According to the system design, a wheelset size measurement system based on MLSL is built, and the parameters of camera, MLSL plane and each measurement module are calibrated, and the three-dimensional measurement model of the system is constructed. The experimental results show that there is a certain deviation between the measurement system and the manual measurement of wheelset parameters, but the overall measurement results of wheelset measurement system are better than those of manual measurement and within the allowable range of measurement error. Among them, the measurement accuracy of wheel diameter and rim width is ±0.2 mm, the measurement accuracy of rim width and height is ±0.25 mm, and the measurement error of QR value is less than 0.25 mm. The intelligent detection system for rail transit vehicle wheelsets combined with SL technology proposed in this paper can effectively adapt to the operation needs of modern rail transit.

When the MLSL detection system measures the wheel diameter, the data collected by the camera system comes from some areas of the wheelset. Therefore, when the out-of-roundness of the wheelset is large, the measurement results have a large deviation. As a result, the acquisition module can be added reasonably to measure the size of the wheel set at different positions, reduce the measurement error of the wheel diameter and measure the out-of-roundness of the wheelset.

Although the wheel detection data acquisition system in this paper combines intelligent methods, it does not set up an adaptive algorithm, and structural damage will inevitably occur after a long time of operation. Therefore, it is necessary to introduce an adaptive acquisition system and set up a predictive maintenance system to further improve the intelligent operation ability of the system.

Declarations

All authors declare that they have no conflicts of interest.

References

Bruni, S., Mistry, P.J., Johnson, M.S., Bernasconi, A., Carboni, M., Formaggioni, D., … and Marazzi, I. (2022) 'A vision for a lightweight railway wheelset of the future', *Proceedings of the Institution of Mechanical Engineers, Part F: Journal of Rail and Rapid Transit*, Vol. 236, No. 10, pp.1179–1197.

Fu, W., He, Q., Feng, Q., Li, J., Zheng, F. and Zhang, B. (2023) 'Recent advances in wayside railway wheel flat detection techniques: a review', *Sensors*, Vol. 23, No. 8, pp.3916–3925.

Guedes, A., Silva, R., Ribeiro, D., Vale, C., Mosleh, A., Montenegro, P. and Meixedo, A. (2023) 'Detection of wheel polygonization based on wayside monitoring and artificial intelligence', *Sensors*, Vol. 23, No. 4, pp.2188–2198.

Guo, X., Ji, Z., Feng, Q., Wang, H., Yang, Y. and Li, Z. (2022) 'URS: a light-weight segmentation model for train wheelset monitoring', *IEEE Transactions on Intelligent Transportation Systems*, Vol. 24, No. 7, pp.7707–7716.

He, Y., Liu, D., Zeng, Y., Lu, Q., Yao, S. and Yuan, Y. (2022) 'Research on the recognition method of the axle end mark of a train wheelset based on machine vision', *International Journal of Computational Intelligence Systems*, Vol. 15, No. 1, pp.112–123.

Jwo, J.S., Lin, C.S., Lee, C.H., Zhang, L. and Huang, S.M. (2021) 'Intelligent system for railway wheelset press-fit inspection using deep learning', *Applied Sciences*, Vol. 11, No. 17, pp.8243–8255.

Kaliorakis, N., Sakellariou, J.S. and Fassois, S.D. (2023) 'On-board random vibration-based robust detection of railway hollow worn wheels under varying traveling speeds', *Machines*, Vol. 11, No. 10, pp.933–943.

Li, H., Wang, H., Xie, Z. and He, M. (2022) 'Fault diagnosis of railway freight car wheelset based on deep belief network and cuckoo search algorithm', *Proceedings of the Institution of Mechanical Engineers, Part F: Journal of Rail and Rapid Transit*, Vol. 236, No. 5, pp.501–510.

Lourenço, A., Ribeiro, D., Fernandes, M. and Marreiros, G. (2024) 'Time series data mining for railway wheel and track monitoring: a survey', *Neural Computing and Applications*, Vol. 36, No. 27, pp.16707–16725.

Mohammadi, M., Mosleh, A., Vale, C., Ribeiro, D., Montenegro, P. and Meixedo, A. (2023) 'An unsupervised learning approach for wayside train wheel flat detection', *Sensors*, Vol. 23, No. 4, pp.1910–1923.

Mosleh, A., Mohammadi, M., Vale, C., Ribeiro, D., Montenegro, P. and Meixedo, A. (2023) 'Smart detection of wheel defects using artificial intelligence and wayside monitoring system', *International Journal of Railway Research*, Vol. 10, No. 2, pp.9–18.

Peng, X., Zeng, J., Wang, J., Li, D. and Wang, Q. (2023a) 'Wayside wheelset lateral motion detection and vehicle hunting instability evaluation', *Measurement Science and Technology*, Vol. 34, No. 12, pp.125904–125915.

Peng, X., Zeng, J., Wang, Q. and Zhu, H. (2023b) 'Research on an identification method for wheelset coaxial wheel diameter difference based on trackside wheelset lateral movement detection', *Sensors*, Vol. 23, No. 13, pp.5803–5814.

Ren, Z., Yin, Y. and Gao, J. (2022) 'Intelligent identification of mortar void in ballastless slab track using the wheelset acceleration combined with CNN-SVM', *Journal of Mechanical Science and Technology*, Vol. 36, No. 12, pp.5845–5857.

Shaikh, M.Z., Ahmed, Z., Chowdhry, B.S., Baro, E.N., Hussain, T., Uqaili, M.A., … and Shah, A.A. (2023) 'State-of-the-art wayside condition monitoring systems for railway wheels: a comprehensive review', *IEEE Access*, Vol. 11, No. 1, pp.13257–13279.

Song, Y., Ji, Z., Guo, X., Hsu, Y., Feng, Q. and Yin, S. (2024) 'A comprehensive laser image dataset for real-time measurement of wheelset geometric parameters', *Scientific Data*, Vol. 11, No. 1, pp.462–473.

Su, X., Zhao, G., Sun, Y. and Li, N. (2024) 'Data-driven intelligent detection model of railway vehicle wheels flat', *Latin American Journal of Solids and Structures*, Vol. 21, No. 1, pp.e526–e535.

Sun, J., Meli, E., Song, X., Chi, M., Jiao, W. and Jiang, Y. (2023) 'A novel measuring system for high-speed railway vehicles hunting monitoring able to predict wheelset motion and wheel/rail contact characteristics', *Vehicle System Dynamics*, Vol. 61, No. 6, pp.1621–1643.

Velletrani, F., Licciardello, R. and Bruner, M. (2020) 'Intelligent wheelsets for the trains of the future. The role of in-service wheel-rail force measurement' [Sale montate intelligenti per il treno del futuro. Il ruolo della misura in esercizio delle forze ruota-rotaia], *Ingegneria Ferroviaria*, Vol. 75, No. 10, pp.701–725.

Vrba, J. (2023) 'Cooperation of active steering control of wheelsets with subsystems of an autonomous urban rail vehicle', *Acta Polytechnica CTU Proceedings*, Vol. 43, pp.117–125.

Zhu, W., Xiao, X., Huang, Z. and Fan, W. (2020) 'Evaluating the wheelset health status of rail transit vehicles: synthesis of wear mechanism and data-driven analysis', *Journal of Transportation Engineering, Part A: Systems*, Vol. 146, No. 12, pp.04020139–04020150.